Deep Learning Based Hybrid Beamforming for mmWave Dual-Functional Radar-Communication

Xiaoyou Yu, *Member, IEEE,* Tianchu Li, Ziyun Tian, and Miao Yu

***Abstract*—In the vehicle-to-everything (V2X) application scenario, we propose a novel deep learning (DL) based Hybrid beamforming (HBF) design for the dual-functional radar-communication (DFRC) system with the millimeter wave (mmWave) massive multiple-in-multiple-output (MIMO) architecture, which enables real-time data exchange and environmental perception. Crucially, the numerical simulations reveal a significant reduction in bit error rate (BER), from 10^{-5} to 10^{-7} at the signal-to-noise ratio (SNR) of 0 dB compared to alternative algorithms, underscoring its superiority in ensuring data integrity and reliability during transmission. This reduction in BER, alongside the 1 dB gain in sum-rate and 3 dB improvement in rad-com tradeoff beampattern, underscores the comprehensive advantages of our DL-based HBF design for DFRC systems over existing HBF designs, which provides robust support for future intelligent transportation systems.**

Link to graphical and video abstracts, and to code: https://latamt.ieeer9.org/index.php/transactions/article/view/8910

***Index Terms*—Hybrid beamforming (HBF), Dual-functional Radar-communication (DFRC), Millimeter wave (mmWave), multiuser multiple input multiple output (MU–MIMO), Deep Learning (DL), Convolutional neural networks (CNN), Sum Mean Square Error (sum-MSE), Bit Error Rate (BER)**

I. INTRODUCTION

Dual-functional radar-communication (DFRC) systems can simultaneously enable cooperative communication and radar sensing, which is crucial to such applications as vehicle-to-everything (V2X) in the sixth-generation mobile communication (6G) era [1]–[4]. Meanwhile, as a promising technology for a joint radar and communication system, HBF has been extensively studied for trade-offs between radar and communications performance ([1], [4], [5]).

There is a lot of deep research on related works of HBF for MIMO systems, especially Multi-User Multiple-Input Multiple-Output (MU-MIMO) systems, in which a base station communicates with multiple users simultaneously at the same time. [6] presents the performance evaluation of an amplify-and-forward (AF) relay-assisted MU–MIMO downlink transmission system for correlated fading channels. [7] presents two precoding techniques for a reconfigurable intelligent surface (RIS)-assisted MU-MIMO double quadrature spatial modulation (DQSM) downlink transmission system. Recently, deep learning (DL) with well well-trained convolutional neural network (CNN) provided a new train of thought for HBF design in mmWave MIMO systems [8]–[11]. Literature [8] presents a dynamic partially connected (DPC) structure-based CNN hybrid precoding with a multi-user optimization algorithm. An innovative DL-based hybrid precoding approach is developed in [9] to maximize spectral efficiency (SE). DL can conduct feature learning and hierarchical feature extraction from data/signal sets [10]. However, the DL-based algorithms do not consider radar sensing functions. Although [11] investigates a DL-based optimization approach for joint radar and communication (JRC) beamforming to enhance the SE for communication users and guarantee the probability of detecting targets, the study has only considered perfect channel state information(CSI), which is not appropriate in real scenarios [12]. It is necessary to seek a low-complexity and efficient algorithm.

Based on the above literature analysis, we hope the DFRC system can be robust to imperfect CSI, as the channel environment is often the case under Telematics systems. In addition, to get a better HBF design, we try to improve the performance of the CNN algorithm including the radar sensing function as a constraint. Furthermore, we would like to improve the computational speed of the CNN neural network and be able to analyze all possible HBF design combinations based on a large amount of data. The contributions of this paper are as follows:

- A novel HBF design is proposed for the DFRC system minimizing the sum-MSE of multi-user downlinks while simultaneously satisfying a well-designed radar beampattern. The proposed scheme is very close to the performance of an ideal HBF scheme and possesses a 3 dB performance advantage over other existing algorithms for radar communication integrated balanced beams.
- The HBF design is derived from a trade-off optimization with penalty terms. An effective solution can be obtained via a CNN-based method using a pre-designed optimal matching search algorithm. The proposed CNN-HBF algorithm provides a better improvement in BER and rate sum compared to other existing algorithms, where an SNR improvement of at least 2 dB and a rate sum improvement of around 1 dB are obtained at a BER of 10^{-4}.
- Sufficient large training data are used to make the CNN

The associate editor coordinating the review of this manuscript and approving it for publication was Carolina Del-Valle-Soto (Corresponding author: Xiaoyou Yu).

This work was supported in part by the National Natural Science Foundation of China under Grant 62232007 and the National Key Research and Development Program of China (Grants Nos.2023YFB3001805).

X. Yu, T. Li, Z. Tian, and M. Yu are with the College of Computer Science and Electronic Engineering, Hunan University, Changsha, China (e-mails: yuxiaoyou@hnu.edu.cn, tianchuli@hnu.edu.cn, tianziy@hnu.edu.cn, and yumiao96@hnu.edu.cn).

method robust to channels with imperfect CSI, which improves the rate sum performance by an average of 5 dB compared to other algorithms at low SNR. Besides, the introduction of the attention mechanism can reduce the computation time by between 75% and 80%.

The remainder of the paper is organized as follows. Section II introduces an HBF based DFRC system at the mmWave band. Section III formulates the tradeoff problem between communications and radar consideration. Section IV develops an HBF design based on the DL framework with CNN. Section V then presents the simulation results with comparative analysis. Finally, Section VI summarizes the paper.

Notation: Throughout the paper: $\mathbf{a}$ and $\mathbf{A}$ denote vectors and matrices, respectively. The conjugate transpose, conjugate, and transpose of a matrix are denoted as $(\cdot)^H$, $(\cdot)^c$ and $(\cdot)^T$. The trace, Frobenius norm of a matrix are represented as $\mathrm{tr}(\cdot)$, $\|\cdot\|_F$, the Euclidean norm of a vector is given as $\|\cdot\|$. And $\mathbf{A}_{(mn)}$ is the (m,n)th entry of a matrix, $\mathbf{A}^\dagger$ is the Moore-Penrose pseudo inverse of $\mathbf{A}$. $\mathbf{I}_n$ denotes the $n \times n$ identity matrix. We use $\mathbb{E}[\cdot]$ for statistical expectation. The $\mathcal{N}\left(\mu, \sigma^2\right)$ is a complex Gaussian random variable with mean μ and variance σ^2.

II. System Model

The application scenario of mmWave DFRC with targets located in the V2X communication environment can be described in Fig. 1. We consider a DFRC system equipped with N_T transmitter antennas array, serving U users (receipt vehicles) in the downlink while sensing N_{tar} target located in the Infrastructure to Vehicles (I2V) communication environment. Each user is equipped with N_R receiver antenna array and both the antenna arrays at the transmitter and receiver are uniform linear array (ULA) antennas. The DFRC system serves multiple users by transmitting a single data stream to each user, i.e., $N_{\mathrm{S}} = 1$ for each user. Thus, it follows $U \leq N_{\mathrm{RF}}$, where N_{RF} is the number of RF chains used in the DFRC system. For simplicity and generality, we define digital beamforming as DBF and analog beamforming as ABF.

A. Channel Model

We assume that the u-th mmWave communication channel (Hu) can be modeled as a cluster channel with a limited number of scattered paths [13].

$$\mathbf{H}_u = \gamma \sum_{i=1}^{N_{\mathrm{cl}}} \sum_{j=1}^{N_{\mathrm{ray}}} \alpha_{ij} g_R\left(\theta_{(ij)}\right) g_T\left(\phi_{(ij)}\right) \mathbf{a}_R\left(\theta_{ij}\right) \mathbf{a}_T^H\left(\phi_{ij}\right), \tag{1}$$

where $\mathbf{a}_T(\phi)$ and $\mathbf{a}_R(\theta)$ represent the steering vector at the road infrastructure (RI) and user equipment (UE), respectively. where $\gamma = \sqrt{N_T N_R / \left(N_{\mathrm{cl}} N_{\mathrm{ray}}\right)}$ represents the normalization factor with N_{cl} being the number of clusters and each of which has N_{ray} paths. N_T and N_R represent the number of antennas at the RI and each user, respectively. α_{ij} denotes the channel gain associated with the ith scattering cluster and the jth path with $i = 1, \cdots, N_{cl}$ and $j = 1, \cdots, N_{ray}$. (θ_{ij}/ϕ_{ij}) is the angle of arrival and departure (AoA/AoD) pair corresponding to a certain path, which satisfies $\phi_{ij} \in [-\pi/2, \pi/2]$ and $\theta_{ij} \in [-\pi/2, \pi/2]$ for later set of the field of view (FoV). $g_R\left(\theta_{(ij)}\right)$ and $g_T\left(\phi_{(ij)}\right)$ are the antenna element gains related with receive and transmit antennas, respectively. $\mathbf{a}_{\mathrm{T}}(\phi_{ij}) \in \mathbb{C}^{N_{\mathrm{T}} \times 1}$ is the array response vector at the transmitter. By assuming the ULA antenna for DFRC system, the nth element of the steering vector $\mathbf{a}_{\mathrm{T}}(\phi_{ij})$ is given as

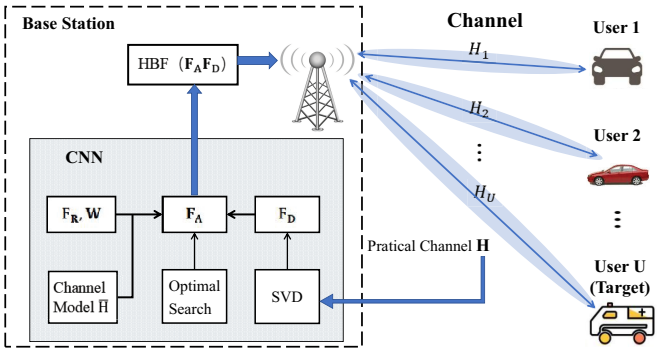

Fig. 1. HBF architecture for mmWave DFRC in V2X.

$$[\mathbf{a}_{\mathrm{T}}(\phi_{ij})]_n = \exp\left\{-\frac{2\pi}{\lambda} p_n \sin\left(\phi_{ij}\right)\right\}, \tag{2}$$

where p_n is the position of the nth antenna element in antenna-axis and λ is wavelength. $\mathbf{a}_R(\theta_{ij})$, the array response vector at the receiver, can be defined in a similar way as (2). Without losing any generality, the first antenna element of $\mathbf{a}_{\mathrm{T}}(\phi_{ij})$ and $\mathbf{a}_R(\theta_{ij})$, respectively, is assumed to be the reference unit for constructing (2).

B. Signal Model

As shown in Fig. 1, the DFRC system applies a low-dimensional DBF $\mathbf{F}_{\mathrm{D}} = [\mathbf{f}_{\mathrm{D1}}, \mathbf{f}_{\mathrm{D2}}, \cdots, \mathbf{f}_{\mathrm{DU}}] \in \mathbb{C}^{N_{\mathrm{RF}} \times U}$ to process the signal streams to be transmitted. Afterward, a high-dimensional ABF $\mathbf{F}_{\mathrm{A}} \in \mathbb{C}^{N_{\mathrm{T}} \times N_{\mathrm{RF}}}$ realizes phase modification of the transmitted signal at the RF front-end via phase shifters. Thus, the transmitted signal by this DFRC system is

$$\mathbf{x} = \mathbf{F}_{\mathrm{A}} \mathbf{F}_{\mathrm{D}} \mathbf{s}, \tag{3}$$

where $\mathbf{s} = [s_1, s_2, \cdots, s_U] \in \mathbb{C}^{U \times 1}$ with $\mathbb{E}\{\mathbf{s}\mathbf{s}^H\} = \mathbf{I}_U$. As the ABF is realized by phase shifters, it is constrained by $\left[[\mathbf{F}_A]_{:,i} [\mathbf{F}_A]_{:,i}^H\right]_{i,i} = 1$. We make the following assumptions:

- The DFRC system uses the same transmit waveform;
- All the users know a priori about mmWave channel $\mathbf{H}$ through pilot symbols at the DFRC system, i.e., perfect CSI.

1) Communication Signal Model: The received signal of the uth user followed by a digital combiner $\mathbf{w}_u \in \mathbb{C}^{N_R \times 1}$ can be viewed as a form with the downlink multi-user interference (MUI) [14], which is formulated as

$$\begin{aligned} y_u &= \mathbf{w}_u^H \mathbf{H}_u \mathbf{x} + \mathbf{w}_u^H \mathbf{n}_u \\ &= \mathbf{w}_u^H \mathbf{H}_u \mathbf{F}_A \mathbf{f}_{Du} \mathbf{s}_u + \mathbf{w}_u^H \mathbf{H}_u \sum_{i \neq u} \mathbf{F}_A \mathbf{f}_{Di} \mathbf{s}_i + \mathbf{w}_u^H \mathbf{n}_u, \end{aligned} \tag{4}$$

where the second statement is MUI for the u-th user, $\mathbf{n}_u \sim \mathcal{CN}\left(\mathbf{0}, \sigma^2 \mathbf{I}_{N_\mathrm{R}}\right)$ is the complex gain additive white Gaussian noise (AWGN) matrix and each item has power of σ^2.

We notice that the power of MUI P_{MUI} directly influences the overall sum-rate [15]. It adds noise to form the interference of effective signal, thus reducing the signal to interference plus noise ratio (SINR), which is given by

$$\Gamma_u = V_u^{-1} G_u, \tag{5}$$

where $G_u = \mathbf{w}_u^H \mathbf{H}_u \mathbf{F}_\mathrm{A} \mathbf{f}_{\mathrm{D}u} \mathbf{f}_{\mathrm{D}u}^H \mathbf{F}_\mathrm{A}^H \mathbf{H}_u^H \mathbf{w}_u$ is power of signal with $\mathbf{f}_{\mathrm{D}u}$ being the sub-column of $\mathbf{F}_\mathrm{D}$ corresponding to the uth user. $V_u = P_{\mathrm{MUI}u} + P_{\mathbf{n}u}$ is the covariance matrix summed by the power of MUI and the channel noise, wherein the power of MUI $P_{\mathrm{MUI}u} = \sum_{i \neq u}^{U} \mathbf{w}_u^H \mathbf{H}_u \mathbf{F}_\mathrm{A} \mathbf{f}_{\mathrm{D}i} \mathbf{f}_{\mathrm{D}i}^H \mathbf{F}_\mathrm{A}^H \mathbf{H}_u^H \mathbf{w}_u$ and the power of noise $P_{\mathbf{n}u} = \sigma^2 \mathbf{w}_u^H \mathbf{w}_u$. It follows that the achievable sum-rate of U users can be given as

$$R = \sum_{u=1}^{U} \log_2 \left(1 + \frac{P}{N_\mathrm{S}} \Gamma_u\right). \tag{6}$$

Considering that MSE, which is relevant to the rate R, is a direct performance measure to characterize the transmission reliability, we will use this metric as the standard to measure the performance of subsequent designs of the HBF.

2) Radar Signal Model: Suppose there are N_{tar} targets to be sensed in the communication environment, which are located in angles $[\theta_1, \theta_2, \cdots, \theta_{N_{tar}}]$. We regard the radar targets as the virtual users of downlink communication and assume that the radar channel is a line-of-sight (LOS) channel. Therefore, the radar channel can be expressed as $\mathbf{H}_r = \sum_{n=1}^{Ntar} \alpha_n \mathbf{a}_T(\theta_n) \mathbf{a}_T^T(\theta_n)$. From (3), we note that $\mathbf{F}_\mathrm{A}\mathbf{F}_\mathrm{D}$ can be viewed as the transmit beamspace matrix. The signal radiated towards a target located at θ_n direction can then be modeled as

$$y(\theta_n) = \mathbf{a}_T^T(\theta_n)\mathbf{x} = \mathbf{a}_T^T(\theta_n)\mathbf{F}_\mathrm{A}\mathbf{F}_\mathrm{D}\mathbf{s}. \tag{7}$$

It follows (7) that power $P(\theta_n)$ of transmitting signal can be derived as

$$P(\theta_n) = \mathbf{a}_T^H(\theta_n)\mathbf{F}_\mathrm{A}\mathbf{F}_\mathrm{D}\mathbf{F}_\mathrm{D}^H\mathbf{F}_\mathrm{A}^H\mathbf{a}_T(\theta_n). \tag{8}$$

It can be seen from (8) that the radar sensing purpose of the DFRC system is only concerned with steering vector and beamforming schemes. Once the beamforming $\mathbf{F}_\mathrm{A}\mathbf{F}_\mathrm{D}$ is designed, the energy of transmitting the signal is focused on the direction of interest. Once a beamforming matrix $\mathbf{F}_\mathrm{R}$ corresponding to the desired beampattern is obtained in advance, the HBF $\mathbf{F}_\mathrm{A}\mathbf{F}_\mathrm{D}$ can be designed to approximate $\mathbf{F}_\mathrm{R}$, thus to form closely a desired beampattern, which is given in the following section.

III. Problem Statement

In this section, we study an appropriate HBF to meet the following requirements:

- To minimize the sum-MSE of communication by designing an HBF.
- To formulate a beampattern that matches multiple targets sensing for radar.
- To satisfy the total power constraint at the transmitter side.

We first introduce a desired beampattern design for the MIMO radar-only system to meet the above requirements.

A. Radar Beampattern Metric of the DFRC System

Compared with the traditional phased array radar, orthogonal waveform MIMO radar has a larger virtual array aperture and a higher degree of freedom [16], [17]. The design of the beampattern is equivalent to the design of the covariance matrix of the transmit signal. According to [16], classical convex optimization can solve such a beampattern design. For a MIMO radar-only system, the normalized power $P_R(\theta)$ of probing signal $\mathbf{x}$ corresponding to target at direction θ can be described as

$$P_R(\theta) = \frac{P}{N_\mathrm{S}} \mathbf{a}_T^H(\theta)\mathbf{F}_\mathrm{R}\mathbf{F}_\mathrm{R}^H\mathbf{a}_T(\theta). \tag{9}$$

To make (9) approach a desired radar beampattern $P(\theta)_d$, the authors in [16] formulate it as the following problem

$$\min_{\mathbf{F}_R} |P(\theta)_d - \mathbf{a}_T^H(\theta)\mathbf{F}_\mathrm{R}\mathbf{F}_\mathrm{R}^H\mathbf{a}_T(\theta)|^2. \tag{10}$$

Thus, the design of $\mathbf{F}_\mathrm{R}$ aims at making beampattern $P_R(\theta)$, which is defined in (9) approach to $P_d(\theta)$. Such a convex least-squares problem can be solved by classical convex optimization tools.

B. Sum-MSE Metric of DFRC System

We use the sum-MSE as an important metric to evaluate communication performance. By recalling (4), a symbol estimator denoted by a scalar factor β [18] is given as

$$\begin{aligned}\hat{s}_u =& \beta \mathbf{w}_u^H \mathbf{H}_u \mathbf{F}_A \mathbf{f}_{Du} \mathbf{s}_u + \beta \mathbf{w}_u^H \mathbf{H}_u \sum_{i \neq u} \mathbf{F}_A \mathbf{f}_{Di} \mathbf{s}_i \\ &+ \beta \mathbf{w}_u^H \mathbf{n}_u,\end{aligned} \tag{11}$$

where β is the introduced dynamic inertial parameter that meets $\beta \in [0, 1]$. The first item to the right of the equal sign is the expected receiving signal of the uth user, while the second and the third items represent the MUI and the AWGN. The MSE of the uth user can be defined as $\mathrm{E}\left\{|s_u - \hat{s}_u|^2\right\}$. Thus, the sum-MSE for U users is

$$\mathrm{E}\left\{||\mathbf{s} - \hat{\mathbf{s}}||^2\right\}. \tag{12}$$

The total power of the transmitter satisfies the following constraint

$$\|\mathbf{F}_\mathrm{A}\mathbf{F}_\mathrm{D}\|_F^2 = \mathrm{tr}(\mathbf{F}_\mathrm{A}\mathbf{F}_\mathrm{D}\mathbf{F}_\mathrm{D}^H\mathbf{F}_\mathrm{A}^H) = P. \tag{13}$$

Although the above power constraint also involves two variables, it can be handled flexibly by the formula transformation of β.

C. HBF Design for DFRC System

In order to satisfy both downlink communications and the radar sensing function of the DFRC system, we regard radar targets as virtual users in line-of-sight channels and clusters

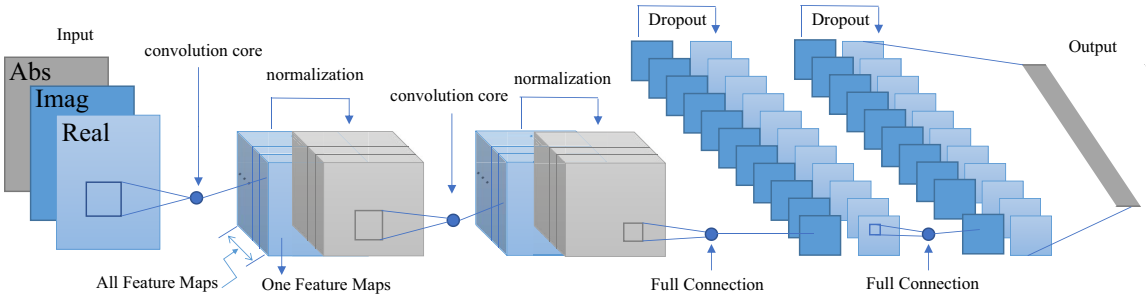

Fig. 2. Block diagram of the CNN for HBF in mmWave DFRC.

contributing to real downlink communications. Specifically, we meet the requirement of the virtual radar user by forming a well-designed beampattern while that of the real communication users by minimizing the sum-MSE defined in (12). Thus, the HBF design can be given as

$$\begin{aligned} &\min_{\mathrm{F_A},\mathbf{F_D},\mathbf{w}_\mu} \mathrm{E}\left\{\|\mathbf{s}-\hat{\mathbf{s}}\|^2\right\} \\ &\text{s.t.} \quad \begin{cases} \|\mathbf{F_A}\mathbf{F_D}-\mathbf{F_R}\|_\mathrm{F} \le \sigma, \\ \mathbf{F_A} \in \mathcal{F}, \\ \mathrm{tr}\left(\mathbf{F_A}\mathbf{F_D}\mathbf{F_D}^H\mathbf{F_A}^H\right) = P, \end{cases} \end{aligned} \tag{14}$$

where $\mathbf{F_R}$ is obtained by solving (10). The first constraint is the consideration of radar beampattern with similarity constraint factor σ. The smaller the σ is, the stricter the radar constraint is. Hence, this work aims to estimate the $\mathbf{F_A}$, $\mathbf{F_D}$ that minimize sum-MSE with constraints of HBF feasibility, transmit power and radar beampattern matching. The first stage of the scheme considers the design of $\mathbf{F_D}$ assuming that $\mathbf{F_A}$ is fixed. With a fixed $\mathbf{F_A}$, the constant modulus constraint in (14) can be removed. This problem can be effectively solved by numerical optimization techniques. Here, the Lagrange functions and Karush-Kuhn-Tucker (KKT) conditions are applied to obtain the optimal solution. The Lagrange function of the problem in (14) is expressed as

$$\begin{aligned} &L\left(\mathrm{F_D},\beta,\lambda,\mu\right) = \mathrm{E}\left\{\|\mathbf{s}-\hat{\mathbf{s}}\|^2\right\} \\ &+\lambda\left[\mathrm{tr}\left(\mathrm{F_A}\ \mathrm{F_D}\ \mathrm{F_D}^H\ \mathrm{F_A}^H\right)-\mathrm{P}\right]+\mu\left[\|\mathrm{F_A}\ \mathrm{F_D}-\mathrm{F_R}\|_F-\sigma\right] \end{aligned}, \tag{15}$$

Where μ is the Lagrangian multiplier associated with the DFRC constraint, i.e. $\mu \ge 0$. λ is a Lagrangian multiplier related to the power constraint. Since it is an equality constraint, there is no range requirement for λ. By differentiating the Lagrangian function and setting the result to zero, the optimal solution can be obtained. According to [19], optimized $\mathbf{F_D}$ can be represented as $\mathbf{F_D} = \beta^{-1}\mathbf{F}_{opt}$, where $\mathbf{F}_{opt}$ is an unconstrained digital beamformer, which is obtained from SVD of channel matrix, and β is related to the transmit power constraint $\mathrm{tr}(\mathbf{F_A}\mathbf{F_D}\mathbf{F_D}^H\mathbf{F_A}^H) = P$. Hence, $\mathbf{F_D}$ has a closed-form solution as

$$\widetilde{\mathbf{F}}_\mathrm{D} = \left(\mathbf{F_A}^H\mathbf{H}^H\mathbf{W}\mathbf{W}^H\mathbf{H}\mathbf{F_A}+\lambda\mathbf{F_A}^H\mathbf{F_A}\right)^{-1}\mathbf{F_A}^H\mathbf{H}^H\mathbf{W}, \tag{16}$$

$$\beta = \sqrt{\mathrm{tr}\left(\mathbf{F_A}\widetilde{\mathbf{F}}_\mathrm{D}\widetilde{\mathbf{F}}_\mathrm{D}^H\mathbf{F_A}^H\right)/P}, \tag{17}$$

where $\mathbf{H} = \left[\mathbf{H}_1^T,\ldots,\mathbf{H}_U^T\right]^T$ is an effective channel matrix of all users, $\lambda = \sigma^2\,\mathrm{tr}\left(\mathbf{W}^H\mathbf{W}\right)/P$ is the Lagrange multiplier, and $\mathbf{W} = \mathrm{blkdiag}\left\{\mathbf{w}_1,\ldots,\mathbf{w}_U\right\}$ is a block diagonal matrix containing all the user's combiners. An effective solution given in [19] is

$$\mathbf{w}_u = \lambda\mathbf{t}, \tag{18}$$

where $\mathbf{T}$ and $\mathbf{J}$ are obtained from a SVD operation that $\beta\mathbf{f}_{\mathrm{Du}}^H\mathbf{F_A}^H\mathbf{H}_u^H = \lambda\mathbf{g}\mathbf{T}^H = \lambda\mathbf{g}_1\mathbf{t}^H$ with $\mathbf{g}_1$ being the first singular value of $\mathbf{g}$ and $\mathbf{t}$ is corresponding singular vector.

By substituting the optimal $\mathbf{F_D}$ into the objective function of (14) and expanding the previous sum-MSE [18], we have

$$||\mathbf{s}-\hat{\mathbf{s}}||^2 = \mathrm{tr}\left(\mathbf{I}_U+\frac{1}{\lambda}\mathbf{W}^H\mathbf{H}\mathbf{F_A}\left(\mathbf{F_A}^H\mathbf{F_A}\right)^{-1}\times\mathbf{F_A}^H\mathbf{H}^H\mathbf{W}\right)^{-1}. \tag{19}$$

The radar beamforming similarity constraint of (14) can be viewed as a penalty item and can be presented as a minimization form such as

$$\min_{\mathbf{F_A}}\ \mathrm{tr}((\widetilde{\mathbf{F}}_\mathrm{A}-\mathbf{F_R})(\widetilde{\mathbf{F}}_\mathrm{A}-\mathbf{F_R})^H), \tag{20}$$

where $\widetilde{\mathbf{F}}_\mathrm{A}$ is a function of $\mathbf{F_A}$ that substitutes (16) into $\mathbf{F_A}\mathbf{F_D}$. Therefore, the objective function (14) can be expressed as

$$\begin{aligned} \min_{\mathbf{F_A}}\ &\rho\,\mathrm{tr}((\mathbf{I}_U+\frac{1}{\lambda}\mathbf{W}^H\mathbf{H}\mathbf{F_A}\left(\mathbf{F_A}^H\mathbf{F_A}\right)^{-1}\times\mathbf{F_A}^H\mathbf{H}^H\mathbf{W}\right)^{-1}) \\ &+(1-\rho)\,\mathrm{tr}((\widetilde{\mathbf{F}}_\mathrm{A}-\mathbf{F_R})(\widetilde{\mathbf{F}}_\mathrm{A}-\mathbf{F_R})^H), \\ &s.t.\ \mathbf{F_A} \in \mathcal{F}. \end{aligned} \tag{21}$$

It is assumed that the angle ϕ_{ij} decides the steering vector $\mathbf{a_T}(\phi_{ij})$. In fact, $\mathbf{F_A}$ is related to linear transformation of $\mathbf{a_T}(\phi_{ij})$, the feasible set $\mathcal{F}$ can be represented as

$$\mathcal{F} = \{\mathcal{F}(1),\mathcal{F}(2),\cdots,\mathcal{F}(S_F)\}, \tag{22}$$

where $N_{path} = \mathrm{num}\{Angle(N_{cl}N_{ray}) \cup Angle(N_{tar})\}$, $\mathcal{F}(s_F) = \{\mathbf{a_T}(\phi_l)\}_{l=1}^{N_{path}}$, representing the number of scatterer angles and radar target angles. According to [20], Vector $a_{TX}\{\phi_l\}$ can be the column of $\mathbf{F_A}$ because $a_{TX}\{\phi_l\}$ is a vector with constant modulus and only phase change. We need to design an optimal matching search algorithm to traverse all nodes from the feasible set $\mathcal{F}$ of $\widetilde{\mathbf{F}}_\mathrm{A}$ to find the optimal solution of s_F satisfying the objective function in (21). By assuming that the angle of the radar target is given randomly from the $\phi_l, l = 1,\cdots,N_{path}$, the steering vector corresponding to the radar target is also included in $\{\mathbf{a_T}(\phi_l)\}_{l=1}^{N_{path}}$. Once the number of paths of all users is given, there are total $S_F = A_{N_{path}}^{N_{RF}}$ possible nodes for searching the optimal s_F, where A denotes permutation operation. Now, the

formula in (21) can be represented as

$$\begin{aligned}\bar{s}_F = &\min_{s_F} \ \rho \operatorname{tr}((\mathbf{I}_U + \frac{1}{\lambda}\mathbf{W}^H\mathbf{H}\mathbf{F}_{\mathrm{A}}\left(\mathbf{F}_{\mathrm{A}}^H\mathbf{F}_{\mathrm{A}}\right)^{-1} \times \mathbf{F}_{\mathrm{A}}^H\mathbf{H}^H\mathbf{W}\Big)^{-1}) \\ &+ (1-\rho)\operatorname{tr}((\widetilde{\mathbf{F}}_{\mathrm{A}} - \mathbf{F}_{\mathrm{R}})(\widetilde{\mathbf{F}}_{\mathrm{A}} - \mathbf{F}_{\mathrm{R}})^H) \\ &s.t. \mathbf{F}_{\mathrm{A}} = \mathcal{F}(s_F),\end{aligned} \tag{23}$$

where $\bar{q}_F$ denotes the optimal node after traversing all nodes that provide the minimum sum-MSE. For the optimal matching search algorithm solving (23), we give the specific steps in Algorithm 1. Different from [14], we consider all possible arrangement combinations of different paths to traverse all nodes from the feasible set $\mathcal{F}$ of $\mathbf{F}_{\mathrm{A}}$ to find the global optimal solution satisfying the objective function in (21). The complexity of the algorithm increases with the number of transmit antennas and scatterers. Besides, obtaining the real-time solution to the problem in (14) is impractical due to the complexity of several matrix variables. To reduce the complexity and the need for the array of responses, in the following sections, we propose a CNN-based approach.

Algorithm 1 Optimal matching search for desired HBF

Input: $\{\mathbf{H_u}\}_{u=1}^{U}$, $\mathbf{F}_{\mathrm{rad}}$, ρ, P
Output: $\mathbf{F}_{\mathrm{A}}, \mathbf{F}_{\mathrm{D}}, \mathbf{W}$
for $1 \le q_F \le Q_F$**:**

$\mathbf{F}_{\mathrm{A}} = \mathcal{F}_{q_F}$;

Initialize $\mathbf{F}_{\mathrm{D}} = \beta^{-1}\mathbf{F}_{\mathrm{opt}}$.

Compute $\mathbf{W}$ according to (18);

Compute $\mathbf{F}_{\mathrm{D}}$ according to (16).

Incorporate radar beampattern constraints as penalty terms in communication objective.

Compute objective function of (23), which is denoted as MSE_{q_F}.

end for q_F**,**

$\bar{q}_F = \arg\min_{q_F} \mathrm{MSE}_{q_F}$.

$\mathbf{F}_{\mathrm{A}} = \mathcal{F}_{\bar{q}_F}$.

IV. Proposed Solution

In this section, we leverage a CNN framework (as shown in Fig. 2) and corresponding training mapping model [21] for solving (23). We assume that the radar targets are a subset of the effective scatterers in the communications channel $\mathbf{H}$. We use Algorithm 1 to get the finite input-and-output pairs for supervised learning of CNN, which provides labels containing optimal $\mathbf{F}_{\mathrm{A}}$ and $\mathbf{F}_{\mathrm{D}}$. We use the classical block-fading channel model as a model of the mmWave channel and use it as the input of CNN. The well-trained CNN provides a nonlinear mapping from the channel matrix $\mathbf{H}$ that contains information of radar reference beamformer $\mathbf{F}_R$ to the analog beamformers $\bar{q}_F$ ($\mathbf{F}_{\mathrm{A}}$), which covers the predicted $\mathbf{F}_{\mathrm{D}}$ obtained by a closed-form solution. Then, the attention mechanism helps the system focus on the heavier analog beamformers $\bar{q}_F$ ($\mathbf{F}_{\mathrm{A}}$) and ignore the parts with lower weights.

A. Deep Neural Network Architecture

The CNN framework consists of at least 10 layers. We take the $3@N_T \times N_R$ channel matrix as the input of the first layer, where 3 means that there are 3 input channels, which is the absolute value of $\mathbf{H}$, in-phase component $\mathcal{R}\{\mathbf{H}\}$ and orthogonal component $\mathcal{I}\{\mathbf{H}\}$. At the same time, the label of supervised learning is obtained by Algorithm 1 to minimize sum-MSE. The label can be denoted as $(\mathbf{X}, \mathbf{z})$, which is the input-output pair. The output layer of CNN is $\mathcal{F}_{\bar{q}_F} \in \mathbb{C}^{N_T \times N_{RF}}$ can be given as $\mathbf{z} = \angle\left\{\mathrm{vec}\left(\mathbf{F}_{\mathrm{A}}\right)^T\right\} \in \mathbb{C}^{N_{\mathrm{T}}N_{\mathrm{RF}}}$, where $\angle$ is an angle conversion function. After the CNN online prediction obtains the required HBF matrix data, $\mathbf{F}_{\mathrm{A}}$ is angularised and converted into angle data. The neural network output is the most available node in the selectable set. The second and fourth layers are convolution layers each with $256@3 \times 3$ filters. The original signal features can be enhanced and the noise can be reduced through convolution operation. Each convolution layer is followed by a normalization layer, and the activation function (modified linear unit Relus) is used to correct the negative number to 0 to normalize the image after convolution. Next, there are two fully connected layers to implement classification, which are located in the sixth layer and the eighth layer, respectively with 1,024 neurons in each layer. After each fully connected layer, a dropout layer is connected with 50% probability, respectively, to prevent overfitting. The complexity of CNN increases with the increase of parameters and layers, which is

$$L_c^2\left(2L_{\mathrm{conv}}(rc+1) + 2(L_{fc}+1) \times \frac{50}{100}\right), \tag{24}$$

where $L_c = 3$ is number of channels, and $L_{conv}@r \times c = 256@3\times3$ represents L_{conv} filters with size of 3×3 in both two convolutional layers. $L_{fc} = 1,024$ is the number of units in each fully connected layer. $\frac{50}{100}$ represents the drop probability of dropout layer. Thus, there are a total of 55,305 parameters in this CNN network.

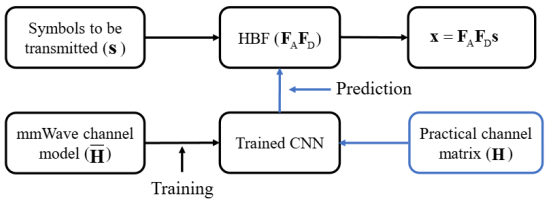

Fig. 3. Offline training and online prediction.

B. Training

The robustness of the user channel is the premise of the performance guarantee for a large-scale mmWave MIMO system. Hence, we must input several synthetic noise interference channels into the CNN network in the training procedure. The offline training and online prediction are shown in Fig. 3.

Specifically, we randomly generate M different channel implementations. After that, we synchronously add N different noise interference terms to each channel. Thus, the SNR of the training data is defined as $\mathrm{SNR}_{\mathrm{TRAIN}} = 20\log_{10}(\frac{|[\mathbf{H}]_{i,j}|^2}{\sigma^2_{\mathrm{TRAIN}}})$. $\sigma^2_{\mathrm{TRAIN}}$ is the variance of synthetic noise. Therefore, the number of training data is $K = M \times N$. The generation of training data $\mathbb{D}$ is summarized in Algorithm 2. The realization of $\mathbf{H}$ includes the channel of all users. In addition, we also introduce synchronization noise to enhance the robustness of subsequent training thus improving the fitness of the imperfect CSI of the channel.

Algorithm 2 Generation of training data for CNN

Input: N_c, N_i, SNR_{TRAIN}.
Output: Training data $\mathbb{D}$

Initialize N_c random mmWave channel matrices $\mathbf{H}_m, m = 1, \cdots, M$, the feasible solution set $\mathcal{F}_m$ of $\mathbf{F}_{\mathrm{A}m}$ is given by the corresponding array steering vector $\mathbf{a}_{\mathrm{T}m}$, $k = 1$.

for $1 \le m \le M$**:**

for $1 \le n \le N$**:**

Add synchronization noise with variance $\sigma^2_{\mathrm{TRAIN}}$ to $\mathbf{H}_n$;

Obtain $\mathbf{F}_{\mathrm{A}}^{m,n} = \mathcal{F}_{\bar{q}_F}^{m,n}$ according to Algorithm 1.

$\left[[\mathbf{X}^{(k)}]_{:,:,1}\right]_{i,j} = \left|[\mathbf{H}^{(m,n)}]_{i,j}\right|$,

$\left[[\mathbf{X}^{(k)}]_{:,:,2}\right]_{i,j} = \mathcal{R}\left\{[\mathbf{H}^{(m,n)}]_{i,j}\right\}$,

$\left[[\mathbf{X}^{(k)}]_{:,:,3}\right]_{i,j} = \mathcal{I}\left\{[\mathbf{H}^{(m,n)}]_{i,j}\right\}$.

$\mathbf{z}^k = \angle\{\mathrm{vec}(\mathbf{F}_{\mathrm{A}}^{(m,n)})^T\}$

k=k+1.

end for n**:**

end for m**:**

Training data is constructed as $\mathbb{D} = (\mathbb{D}^{(1)}, \cdots, \mathbb{D}^{(K)})$.

In particular, we generate $M = 6000$ for $U = 3$ users. 30% and 70% of them are used as validation and training data, respectively. The hyperparameter needs to be set according to the effect of the validation set. The criterion of $N = 100$ adding synchronous noises is given according to $\mathrm{SNR}_{\mathrm{TRAIN}} \in \{10, 20, 30\}$ dB. Different levels of $\mathrm{SNR}_{\mathrm{TRAIN}}$ take into account the different severities of channel damage. The loss function is defined as

$$Loss = \frac{1}{K}\sum_{k=1}^{K}\left(\mathbf{z}^{(k)} - f\left(\mathbf{X}^{(k)}\right)\right)^2, \tag{25}$$

where $f(\mathbf{X})$ represents the nonlinear transformation of $\mathbf{X}$. The stochastic gradient descent (SGD) algorithm is applied in neural networks to alleviate the high computational cost of backpropagation in the whole training set. In simulations with 100 Monte Carlo trials, test data is added with synchronous noise with $\mathrm{SNR}_{\mathrm{TEST}} = 20\log_{10}\left(\frac{|[\mathbf{H}]_{i,j}|^2}{\sigma^2_{\mathrm{TEST}}}\right)$. We set $\mathbf{H}_u$ with $N_{path} = 20$ for each user and $\phi \in [-90°, 90°]$ in Algorithm 1. So the data contains enough randomness to train the corresponding network. The above steps can be simplified as those in Fig. 3. Here, the training order is $N_R \times N_T \times 3 \times M \times N \times \mathrm{len}(\mathrm{SNR}_{\mathrm{TRAIN}})$. We give an example of iteration time in Table I.

TABLE I
ITERATION TIME

epochs	Iteration	time(s)	validation RMSE	Loss
1	1	0	15.86	111.3286
17	50	1	0.81	0.2589
34	100	1	0.33	0.0506
50	150	2	0.31	0.0426
67	200	3	0.30	0.0373
84	250	4	0.29	0.0320

C. Prediction

The purpose of training is to obtain the weight of a neural network, which provides CNN with judgment and prediction power. In order to make the prediction more accurate, the amount of trained data is very large. Therefore, we introduce the attention mechanism to reduce the computational complexity of the prediction phase by biasing the system towards information that is more favorable to judgment.

The attention mechanism is mainly divided into three stages: In the first stage, the practical channel matrix $\mathbf{H}$ is taken as the input, and the similarity score S_i between $\mathbf{H}$ and the channel information $\mathbf{X}^{(k)}$ in the training data $\mathbb{D}^{(k)}$ is calculated. In the second stage, the original score S_i of the first stage is normalized to obtain the weight coefficient a_i. The third stage is the weighted summing of the analog beamforming $\bar{q}_F$ ($\mathbf{F}_{\mathrm{A}}$) according to the weight coefficient.

a_i is also known as the attention distribution, which represents the attention to the ith training data $\mathbb{X}^{(i)}$ based on the input data $\mathbf{H}$. Motivated by [27], the soft attention model can be expressed as

$$a_i = F\left(H, X^{(i)}\right) = \frac{\exp\left(\mathrm{f}\left(H, X^{(i)}\right)\right)}{\sum_{\mathrm{j}=1}^{\mathrm{K}}\exp\left(\mathrm{f}\left(H, X^{(j)}\right)\right)} \tag{26}$$

where the practical input channel matrix H and the channel information $X^{(i)}$ in the training message are the query vector and the key vector in the attention mechanism, respectively. And the scoring function $\mathrm{f}\left(H, X^{(i)}\right)$ can be expressed as

$$\mathrm{f}\left(H, X^{(i)}\right) = \frac{\left(\mathrm{X}^{(\mathrm{i})}\right)^{\mathrm{T}}\mathrm{H}}{\sqrt{\mathrm{d}}}, \tag{27}$$

where d represents the dimension of the key vector. The third stage we need to do is obtaining the important information based on the distribution of attention. At this point, we use a "soft" information selection mechanism to summarize, which can be expressed as

$$\mathrm{att}\left(H, X^{(i)}\right) = \sum_{\mathrm{i}=1}^{\mathrm{K}} a_i \cdot \mathrm{z}^{\mathrm{i}}. \tag{28}$$

Finally, according to the attention mechanism, the system focuses on the parts with heavy weights and predicts the optimal simulated beamforming $\bar{q}_F$ ($\mathbf{F}_{\mathrm{A}}$).

TABLE II
COMPARISON WITH OTHER DESIGN

Ref	mmWave	Functions	BF	way	antennas	Com SE (bps/Hz)	Rad BG (dB)	EE (bps/Hz/J)
[16]	No	Rad	DBF	SQP	16×16	N.G.	7.4	N.G.
[20]	Yes	Com	HBF	OMP	64×16	16.3	N.G.	0.54
[14]	Yes	Com	HBF	Quantized Codebooks	64×16	17	N.G.	0.69
[22]	Yes	Com	HBF	PE-MO	64×16	19.4	N.G.	0.68
[23]	No	Rad-Com	DBF	Lagrangian method	16×4	4	6.2	0.67
[18]	Yes	Com	HBF	MLP	64×16	21.2	N.G.	0.70
[24]	Yes	Com	HBF	two-stage	64×16	20.1	N.G.	0.69
[25]	Yes	Com	HBF	DNN	64×16	21.7	N.G.	0.70
[26]	Yes	Rad-Com	HBF	TAltMin	64×16	14.9	12	0.69
Proposed	Yes	Rad-Com	HBF	CNN	64×16	22.3	14.2	0.71

N.G.: Not given by the reference; BG: Beampattern gain; EE: Energy Efficiency.

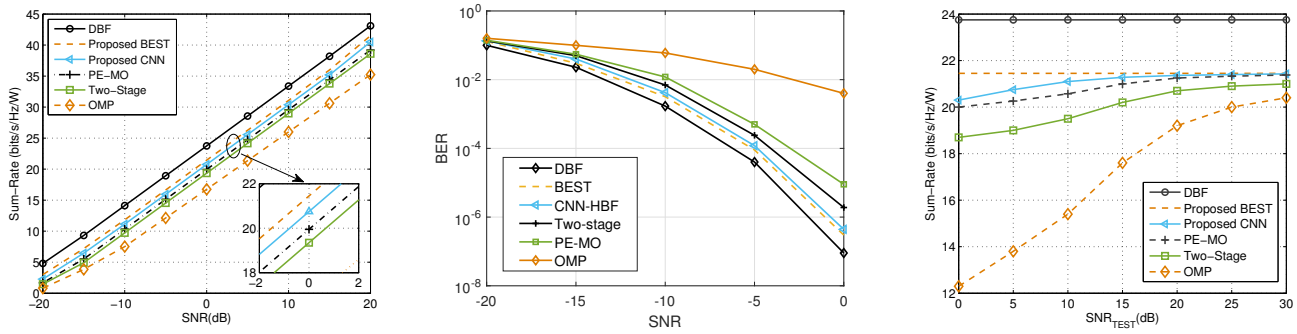

(a) (b) (c)

Fig. 4. (a)Sum-rate vs SNR, (b)BER based on QPSK modulation, (c)Sum-rate vs $\mathrm{SNR}_{\mathrm{TEST}}$.

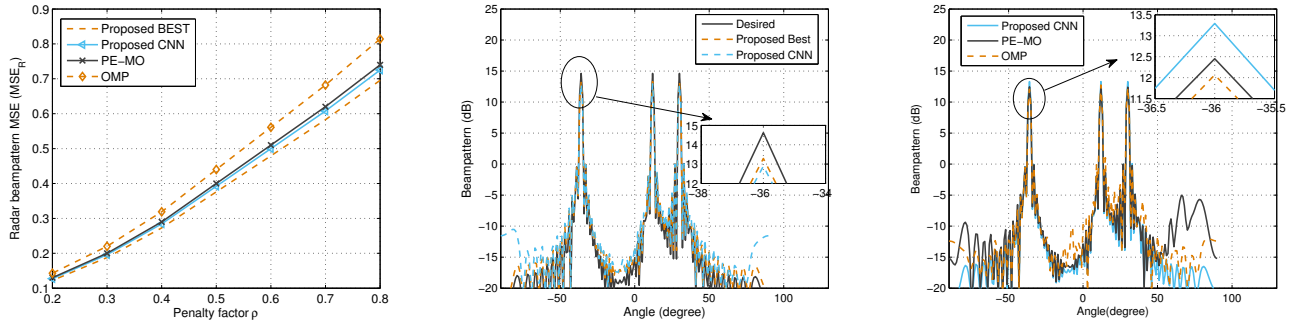

(a) (b) (c)

Fig. 5. (a)Radar beampattern vs penalty factor, (b)Radar beampattern vs desired, (c)Radar beampattern vs other algorithms.

V. RESULTS

In this section, simulation results are given to evaluate the performance of the trained CNN framework called CNN-HBF. We treat the radar constraint as a penalty term into the objective function and set a penalty factor ρ. The performance of radar improves with the increase of ρ. In particular, $\rho = 0$ and $\rho = 1$, represent the communication-only and the radar-only case, respectively. For the CNN training, the parameters are set as $M = 600$, $U = 3$, $N = 100$. The input of CNN is set as $N_T = 64$ and $N_{RF} = U$ for the transmitter, $N_R = 4$ for each user. We model the mmWave channel similar to [13], where we set $N_{\mathrm{path}} = 10$ for each user with Laplacian distributed azimuths of arrival and departure (AoAs and AoDs), which are randomly distributed in the interval of $[-90°, 90°]$. The average power is allocated to every cluster. The angles of the radar targets randomly select three from the

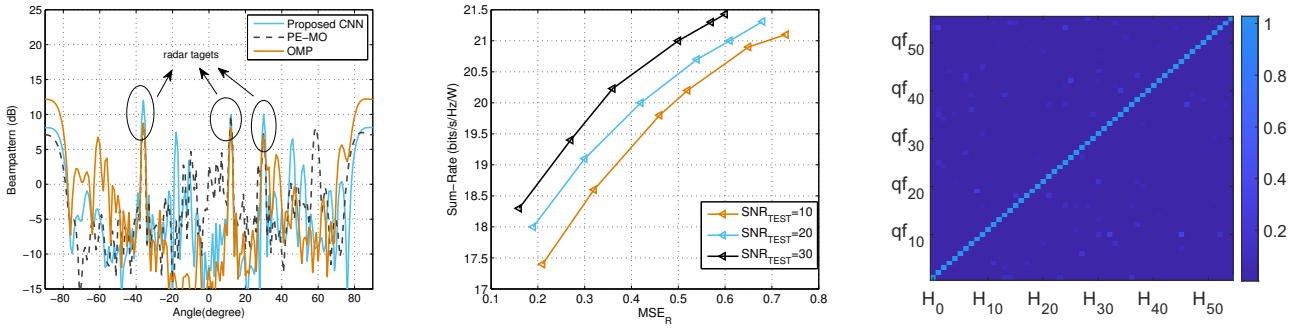

(a) (b) (c)

Fig. 6. Under $N_T = 64$, $N_{RF} = N_S = 3$, (a)Rad-Com tradeoff beampattern, (b)Rad-Com tradeoff between radar beampattern MSE $\mathrm{MSE_R}$ and sum-rate of downlink communication, (c)Attentional mechanism distribution model.

angles of the cluster. This means that radar targets are also contributors to communication path propagation. The learning rate of the SGD algorithm is $r = 0.005$.

The comparisons between the HBF design used in the DFRC system and other similar works are summarized in Table II, where $EE = \frac{R_{rate}}{P_{total}+N_{\mathrm{RF}}P_{\mathrm{RF}}+N_{\mathrm{PS}}P_{\mathrm{PS}}}$, P_{total} is the total power, P_{RF} and P_{PS}, respectively, represent the power of RF chains and phase shifters. Note that $N_{\mathrm{PS}} = N_{\mathrm{T}} \times N_{\mathrm{RF}}$ and $N_{\mathrm{PS}} = N_{\mathrm{T}}$ correspond to full-connected and part-connected MIMO structure, respectively [28]. The EE of hybrid beamforming depends on the efficiency of the signal processing algorithms, the design of the antenna array, and so on. The massive MIMO technique can improve the communication quality without increasing the transmit power, thus indirectly improving EE. More importantly, CNN greatly enhances the efficiency of signal processing algorithms while bringing the output closer to the most optimal solution. In Table II, our proposed method possesses an EE that is not inferior to other methods while balancing the communication and radar performance. The reason why our method achieves higher EE is because we use CNN to solve $\mathbf{F}_{\mathrm{A}}$ compared to other methods. While improving the efficiency of the algorithm, the designed ABF is also closer to the optimal solution. In contrast with other HBF methods, the proposed HBF architecture for the mmWave DFRC system is the most promising way.

A. Downlink Communication Performance

First, we evaluate the spectrum efficiency of communication achieved by proposed design methods of HBF in the DFRC system. Here we set $U = 3$ downlink communication user. Besides, the number of RF chains at the transmitter is equal to $N_{\mathrm{R}} = 4$ as a fully digital combiner is used on the user side. For the transmitter, we set $N_{\mathrm{T}} = 64$ and $N_{\mathrm{s}} = U = 3$, which meets the minimum requirement that $N_{\mathrm{RF}} \geq N_{\mathrm{S}}$ [29]. As the training of CNN is based on Algorithm 1, i.e, $\mathbf{H}$ with no noise, we take the HBF from Algorithm 1 as the 'BEST' case of CNN-HBF. The negative SNR value is introduced to verify the performance of the proposed algorithm in the case of a poor signal-to-noise ratio.

Fig. 4a shows the SE under different SNRs (-20 dB, 20 dB). We compare the performance with $\rho = 0$ of the algorithms with a fixed value of $\mathrm{SNR_{TEST}}$. Obviously, in the process of training CNN, when the synchronization noise is added to the input channel with $\mathrm{SNR_{TEST}} = 10\ dB$, proposed CNN-HBF has a better performance in sum-rate metric as compared to other algorithms [12], [24].

Fig. 4b shows the bit error rate (BER) versus SNR for the proposed CNN-HBF and other methods. Compared to alternative algorithms, a significant reduction in BER can be obtained from 10^{-5} to 10^{-7} at the SNR of 0 dB. In other words, SNR improvement of at least 2 dB and a rate sum improvement of around 1 dB are obtained at BER of 10^{-4}. The curves are consistent with the previous analysis.

Fig. 4c represents the results of the performance of sum-rate versus different numbers of $\mathrm{SNR_{TEST}}$. This represents the robustness of different algorithms to channel destruction. Among them, 'DBF' represents the situation without interference, and 'BEST' denotes a channel that is not destroyed, which is the sum rate obtained from Algorithm 1. As can be seen, the CNN-HBF scheme is more robust.

B. Radar Beampattern Performance

In the process of CNN training, we regard radar targets as the identifiable scatterers contributing to the downlink communication under the angle extracted from $[-90°, 90°]$ with quantification of $5°$. We mainly compare the anti-jamming performance of the three algorithms, i.e, CNN-HBF, PE-MO, and OMP methods [30] under $N_T = 64$, $N_{RF} = N_S = 3$, $\mathrm{SNR_{TEST}} = 20\ dB$.

Fig. 5a shows the impact of penalty factor on radar beampattern MSE, which is defined as $\sum_{n=1}^{N_{tar}} \left(G_{\mathrm{d}}\left(\theta_n\right) - G_{\mathrm{DFRC}}\left(\theta_n\right)\right)^2$ according to [31], G_{d} is defined as (10) to represent the ideal beam pattern formed by the DFRC system for the target to be sensed. G_{DFRC} denotes the beampatterns formulated by the DFRC system. The proposed algorithm radar beampattern is superior to OMP and similar to PE-MO.

Fig. 5b shows that the transmit beampattern of the proposed cnn-HBF based on directional radar pattern design compares with the desired radar pattern obtained by classic Least-Squares techniques [17]. It can be seen that the proposed algorithm is close to the best case.

Fig. 5c shows that the robustness of the CNN method is better than the PE-MO and OMP methods.

C. Radar-Communication Tradeoff Performance

In this subsection, we set different weighted factors ρ to denote a tradeoff between communication and radar functions.

In Fig. 6a, we show the performance of radar beampattern with $\rho = 0.5$. Since the radar target is included in the scatterers and the angle gain assigned to each scatterer satisfies the uniform distribution of $[0, 1]$, the tradeoff beampattern highlights energy concentration on three radar targets. The tradeoff beampattern highlights energy concentration of the proposed algorithm is better than the OMP and PE-MO algorithms.

In Fig. 6b, we display a more intuitive tradeoff between radar beampattern mean squared error ($\mathrm{MSE_R}$) and communication sum-MSE. For the fixed radar beampattern MSE, the sum rate of communications improves with the increase of $\mathrm{SNR_{TEST}}$.

Fig. 6c shows the attention distribution probability of the part of the simulated beamforming and the practical channel matrix with an obvious correspondence. It can be seen that a particular channel matrix is only highly correlated with the corresponding analog beamformer.

TABLE III
PERFORMANCE LOSS FOR HBF DESIGN

Algorithm	N_S	γ_F	Time(s)
Proposed CNN	1	0.012	0.020
	2	0.009	0.022
	3	0.006	0.025
CNN Without Atttenion	1	0.010	0.095
	2	0.008	0.101
	3	0.005	0.981
PE-Mo	1	0.032	0.850
	2	0.019	0.915
	3	0.008	0.920
OMP	1	0.032	8.305
	2	0.032	8.305
	3	0.025	8.578

D. Comparison for HBF Cost Function and Computation Time

In order to further study the effect of the proposed algorithm on the design performance of the beamformers, a cost function is used to measure the approximation between the hybrid beamformer estimated by the algorithm and the unconstrained beamformer. The error between the unconstrained precoder $F_A F_D$ and the estimated precoder F_{opt} is defined as $\gamma_F = \left\| F_{opt} - F_A F_D \right\|_F / \left(N_T N_s \right)$. In Table III, error effects of three hybrid beamforming algorithms are listed in the case of $N_S = \{1, 2, 3\}, \mathrm{U} = 3, N_{TX} = 64, N_{RX} = 4, N_{RF} = 3, \mathrm{SNR_{TEST}} = 20$ dB. As can be seen from Table III, compared with other algorithms, the error of the algorithm based on the CNN precoder is smaller with a faster computing speed.

VI. CONCLUSION

In this paper, we investigate a CNN-HBF design using a DL framework. The simulation results indicate that at least 2 dB SNR gain is obtained compared to other methods at the same BER. At the same time, the method improves the sum rate of at least 1 bit/s/Hz/W over the existing algorithms at the same SNR. The sum rate is stabilized at 20-22 bit/s/Hz/W when the channel interference power is increasing, and the algorithm is robust to channel interference. And the radar communication compromise beam map outperforms other algorithms and is closest to the best case. In future work, we can further consider the performance metrics on the radar side to optimize the beam design as a way to adapt to the needs of radar communication application scenarios such as Telematics.

REFERENCES

[1] X. Yu, Q. Yang, Z. Xiao, H. Chen, V. Havyarimana, and Z. Han, "A precoding approach for dual-functional radar-communication system with one-bit dacs," *IEEE Journal on Selected Areas in Communications*, vol. 40, no. 6, pp. 1965–1977, 2022, doi: 10.1109/JSAC.2022.3155532.

[2] X. Yu, L. Tu, Q. Yang, M. Yu, Z. Xiao, and Y. Zhu, "Hybrid beamforming in mmwave massive mimo for iov with dual-functional radar communication," *IEEE Transactions on Vehicular Technology*, vol. 72, no. 7, pp. 9017–9030, 2023, doi: 10.1109/TVT.2023.3247747.

[3] B. Liu, J. Liu, and N. Kato, "Optimal beamformer design for millimeter wave dual-functional radar-communication based v2x systems," *IEEE Journal on Selected Areas in Communications*, vol. 40, no. 10, pp. 2980–2993, 2022, doi: 10.1109/JSAC.2022.3196089.

[4] F. Maciel, J. Sanchez, L. Soriano, F. Soria, and J. Flores, "User scheduling algorithms in multiuser massive mimo systems towards 5g," *IEEE Latin America Transactions*, vol. 13, no. 12, pp. 3781–3787, 2015, doi: 10.1109/TLA.2015.7404908.

[5] T. Lin and Y. Zhu, "Beamforming design for large-scale antenna arrays using deep learning," *IEEE Wireless Communications Letters*, vol. 9, no. 1, pp. 103–107, 2020, doi: 10.1109/LWC.2019.2943466.

[6] F. R. Castillo-Soria, C. Gutierrez, F. M. Maciel-Barboza, V. I. Rodriguez Abdala, and J. Datta, "Relay-assisted multiuser mimo-dqsm system for correlated fading channels," *ETRI Journal*, vol. 46, no. 2, pp. 184–193, 2024, doi: 10.4218/etrij.2022-0391.

[7] F. R. Castillo-Soria, J. A. Del Puerto-Flores, C. A. Azurdia-Meza, V. Babu Kumaravelu, J. Simón, and C. A. Gutierrez, "Precoding for ris-assisted multi-user mimo-dqsm transmission systems," *Future Internet*, vol. 15, no. 9, p. 299, 2023, doi: 10.3390/fi15090299.

[8] F. Liu, Z. Duan, L. Zhang, B. Shi, Y. Liu, and R. Du, "Dpc-cnn algorithm for multiuser hybrid precoding with dynamic structure," *IEEE Transactions on Green Communications and Networking*, pp. 1–1, 2024, doi: 10.1109/TGCN.2024.3376571.

[9] F. Liu, X. Li, X. Yang, H. Shi, B. Shi, and R. Du, "Deep learning based joint hybrid precoding and combining design for mmwave mimo systems," *IEEE Systems Journal*, vol. 18, no. 1, pp. 560–567, 2024.

[10] A. M. Elbir and K. V. Mishra, "Joint antenna selection and hybrid beamformer design using unquantized and quantized deep learning networks," *IEEE Transactions on Wireless Communications*, vol. 19, no. 3, pp. 1677–1688, 2020, doi: 10.1109/TWC.2019.2956146.

[11] R. Yang, Z. Zhu, J. Zhang, S. Xu, C. Li, Y. Huang, and L. Yang, "Deep learning-based joint transmit beamforming for dual-functional radar-communication system," *IEEE Transactions on Wireless Communications*, pp. 1–1, 2024.

[12] Z. Cheng, B. Liao, and Z. He, "Hybrid transceiver design for dual-functional radar-communication system," in *2020 IEEE 11th Sensor Array and Multichannel Signal Processing Workshop (SAM)*, 2020, pp. 1–5, doi: 10.1109/SAM48682.2020.9104387.

[13] D. Zhang, Y. Wang, X. Li, and W. Xiang, "Hybridly connected structure for hybrid beamforming in mmwave massive mimo systems," *IEEE Transactions on Communications*, vol. 66, no. 2, pp. 662–674, 2018, doi: 10.1109/TCOMM.2017.2756882.

[14] A. Alkhateeb, G. Leus, and R. W. Heath, "Limited feedback hybrid precoding for multi-user millimeter wave systems," *IEEE Transactions on Wireless Communications*, vol. 14, no. 11, pp. 6481–6494, 2015, doi: 10.1109/TWC.2015.2455980.

[15] L. Liang, W. Xu, and X. Dong, "Low-complexity hybrid precoding in massive multiuser mimo systems," *IEEE Wireless Communications Letters*, vol. 3, no. 6, pp. 653–656, 2014, doi: 10.1109/LWC.2014.2363831.

[16] P. Stoica, J. Li, and Y. Xie, "On probing signal design for mimo radar," *IEEE Transactions on Signal Processing*, vol. 55, no. 8, pp. 4151–4161, 2007, doi: 10.1109/TSP.2007.894398.

[17] D. R. Fuhrmann and G. San Antonio, "Transmit beamforming for mimo radar systems using signal cross-correlation," *IEEE Transactions on Aerospace and Electronic Systems*, vol. 44, no. 1, pp. 171–186, 2008, doi: 10.1109/TAES.2008.4516997.

[18] T. Lin, J. Cong, Y. Zhu, J. Zhang, and K. Ben Letaief, "Hybrid beamforming for millimeter wave systems using the mmse criterion," *IEEE Transactions on Communications*, vol. 67, no. 5, pp. 3693–3708, 2019, doi: 10.1109/TCOMM.2019.2893632.

[19] J. Cong, T. Lin, and Y. Zhu, "Hybrid mmse beamforming for multiuser millimeter-wave communication systems," *IEEE Communications Letters*, vol. 22, no. 11, pp. 2390–2393, 2018, doi: 10.1109/LCOMM.2018.2869329.

[20] O. E. Ayach, S. Rajagopal, S. Abu-Surra, Z. Pi, and R. W. Heath, "Spatially sparse precoding in millimeter wave mimo systems," *IEEE Transactions on Wireless Communications*, vol. 13, no. 3, pp. 1499–1513, 2014, doi: 10.1109/TWC.2014.011714.130846.

[21] A. M. Elbir, "Cnn-based precoder and combiner design in mmwave mimo systems," *IEEE Communications Letters*, vol. 23, no. 7, pp. 1240–1243, 2019, doi: 10.1109/LCOMM.2019.2915977.

[22] Z. Xu, S. Han, Z. Pan, and I. Chih-Lin, "Alternating beamforming methods for hybrid analog and digital mimo transmission," in *2015 IEEE International Conference on Communications (ICC)*, 2015, pp. 1595–1600, doi: 10.1109/ICC.2015.7248552.

[23] F. Liu, L. Zhou, C. Masouros, A. Li, W. Luo, and A. Petropulu, "Toward dual-functional radar-communication systems: Optimal waveform design," *IEEE Transactions on Signal Processing*, vol. 66, no. 16, pp. 4264–4279, 2018, doi: 10.1109/TSP.2018.2847648.

[24] A. Alkhateeb, R. W. Heath, and G. Leus, "Achievable rates of multi-user millimeter wave systems with hybrid precoding," in *2015 IEEE International Conference on Communication Workshop (ICCW)*, 2015, pp. 1232–1237, doi: 10.1109/ICCW.2015.7247346.

[25] H. Huang, Y. Song, J. Yang, G. Gui, and F. Adachi, "Deep-learning-based millimeter-wave massive mimo for hybrid precoding," *IEEE Transactions on Vehicular Technology*, vol. 68, no. 3, pp. 3027–3032, 2019.

[26] F. Liu and C. Masouros, "Hybrid beamforming with sub-arrayed mimo radar: Enabling joint sensing and communication at mmwave band," in *ICASSP 2019 - 2019 IEEE International Conference on Acoustics, Speech and Signal Processing (ICASSP)*, 2019, pp. 7770–7774, doi: 10.1109/ICASSP.2019.8683591.

[27] D. Bahdanau, K. Cho, and Y. Bengio, "Neural machine translation by jointly learning to align and translate," *Computer Science*, 2014, doi: 10.48550/arXiv.1409.0473.

[28] L. Zhu, Z. Xiao, X.-G. Xia, and D. Oliver Wu, "Millimeter-wave communications with non-orthogonal multiple access for b5g/6g," *IEEE Access*, vol. 7, pp. 116 123–116 132, 2019, doi: 10.1109/ACCESS.2019.2935169.

[29] E. Zhang and C. Huang, "On achieving optimal rate of digital precoder by rf-baseband codesign for mimo systems," in *2014 IEEE 80th Vehicular Technology Conference (VTC2014-Fall)*, 2014, pp. 1–5, doi: 10.1109/VTCFall.2014.6966076.

[30] B. Li, J. Qiao, Z. Lu, X. Yu, J. Song, B. Lin, and X. Li, "Influence of sweep interference on satellite navigation time-domain anti-jamming," *Frontiers in Physics*, vol. 10, p. 1307, 2023, doi: 10.3389/fphy.2022.1063474.

[31] F. Liu, C. Masouros, A. Li, H. Sun, and L. Hanzo, "Mu-mimo communications with mimo radar: From co-existence to joint transmission," *IEEE Transactions on Wireless Communications*, vol. 17, no. 4, pp. 2755–2770, 2018, doi: 10.1109/TWC.2018.2803045.

Xiaoyou Yu (M'21) received the M.S. and Ph.D. degrees in information and communication engineering from National University of Defense Technology, China, in 1995 and 1998, respectively. He is an A./Prof. at the College of Information Science and Electronic Engineering, Hunan University, China, and a part-time Research Fellow at Advanced Technology Institute. His research interests include array signal processing, dual-function radar-communication, radar and communication coexistence, integrated sensing and communications, anti-jamming, mobile computing, Internet of Vehicles and intelligent transportation systems, artificial intelligence, and its application to signal processing.

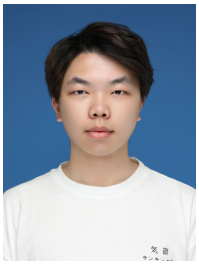

Tianchu Li was born in Changsha, Hunan, China, in 1999. He received a bachelor's degree in communication engineering from Hunan University, Changsha, China, in 2021. He is currently pursuing an M.S. degree at the College of Computer Science and Electronic Engineering, Hunan University. Her research interests include radar communication integration systems.

Ziyun Tian was born in Changsha, Hunan, China, in 1996. She received her bachelor's degree in Internet of Things engineering from Jiangxi University of Finance and Economics, Nanchang, China, in 2021. She is currently pursuing an M.S. degree in the College of Computer Science and Electronic Engineering at Hunan University. Her research interests include integrated sensing and communication systems.

Miao Yu was born in Changsha, Hunan, China, in 1996. She received her bachelor's degree in communication engineering from Hunan Normal University, Changsha, China, in 2018. She is currently pursuing an M.S. degree in the College of Computer Science and Electronic Engineering, at Hunan University. Her research interests include radar communication integration systems.